



ELSEVIER

Contents lists available at ScienceDirect

Materials Research Bulletin

journal homepage: www.elsevier.com/locate/matresbu

Novel palladium-guanine-reduced graphene oxide nanocomposite as efficient electrocatalyst for methanol oxidation reaction

Jen Chao Ng^a, Chou Yong Tan^{a,b,c,*}, Boon Hoong Ong^d, Atsunori Matsuda^e, Wan Jeffrey Basirun^f, Wai Kian Tan^e, Ramesh Singh^a, Boon Kar Yap^{b,g}

^a Department of Mechanical Engineering, Faculty of Engineering, University of Malaya, 50603 Kuala Lumpur, Malaysia

^b International School of Advanced Materials, School of Materials Science and Engineering, South China University of Technology, 510640 Guangzhou, China

^c School of Mechanics, Civil Engineering and Architecture, Northwestern Polytechnical University, China

^d Nanotechnology & Catalysis Research Centre, University of Malaya, 50603 Kuala Lumpur, Malaysia

^e Department of Electrical & Electronic Information Engineering, Toyohashi University of Technology, Toyohashi, Aichi 441-8580, Japan

^f Department of Chemistry, Faculty of Science, University of Malaya, 50603 Kuala Lumpur, Malaysia

^g Department of Electronics and Communication, College of Engineering, Universiti Tenaga Nasional, Km-7, Jalan Ikram-UNITEN, 43009 Kajang, Selangor, Malaysia

ARTICLE INFO

Keywords:

- A. Graphene
- A. Palladium nanoparticles
- A. Guanine
- B. Noncovalent functionalization
- D. Methanol oxidation reaction

ABSTRACT

The agglomeration of metal catalysts can limit the performance of fuel cells. Herein, an easy, scalable, one-pot microwave-assisted method is proposed to introduce guanine, which is a nucleobase found in deoxyribonucleic acid and ribonucleic acid, to the reduced graphene oxide-supported palladium via noncovalent functionalization. Considering the abundant amino, amide, and imino functional groups of guanine that act as anchoring sites, palladium nanoparticles of various shapes such as triangular, rectangular, circular, and diamond are uniformly distributed. The guanine itself is revealed to be catalytically active toward methanol oxidation reaction, serving as second catalyst. Consequently, the as-produced nanocomposite has a larger electrochemically active surface area ($111.98 \text{ m}^2 \text{ g}^{-1}$ vs. $63.80 \text{ m}^2 \text{ g}^{-1}$), greater methanol electro-oxidation ability ($1017.42 \text{ mA mg}^{-1}$ vs. $359.80 \text{ mA mg}^{-1}$), and higher stability in alkaline medium than its counterpart without guanine.

1. Introduction

Direct methanol fuel cells (DMFCs) emerge as alternative low-temperature environmental benign energy source for portable electronic devices that use methanol solution or steam as fuel at anode [1,2]. Its popularity can be ascribed to the merits of methanol, including high theoretical energy density, economical price, and its physical state (liquid form at ambient temperature and pressure) that allows easy transportation and distribution [3,4]. Catalysts are imperative in decreasing the activation energy of the reactions at electrodes. Nonetheless, they occupy approximately 30%–50% of the total cost of fuel cells [5]. Palladium (Pd) nanoparticles (NPs) have been reported as potential substitute of the current commercially used catalyst, platinum (Pt), due to their good resistance to carbon monoxide (CO) poisoning, at least 50 times more abundant on earth, and less cost [6]. Nevertheless, regardless of the types, all catalyst NPs at nano-size can irreversibly agglomerate to reduce the surface energy and thus limit the electrochemical performance [7].

Anchoring metal catalysts on catalyst supports have been

discovered as a wise strategy to prevent catalyst conglomeration [6]. Graphene stands up to be superior among all catalyst supports. Ample reviews and studies on graphene and graphene-related materials have been devoted since its discovery in year 2004 [8,9]. On top of its role in limiting the agglomeration, graphene also facilitates electron and mass transport [7]. Graphene is also endowed with exceptional properties such as large surface area ($2630 \text{ m}^2 \text{ g}^{-1}$), high electrical conductivity (10^5 – 10^6 Sm^{-1}), and excellent thermal conductivity (5300 W/mK), because of its two-dimensional one-atom thickness [10,11]. Graphene oxide (GO) has been the preferred derivative of graphene due to its easy, economical, and scalable production. The oxygen-functional groups, for example hydroxyl ($-\text{OH}$), carboxyl ($-\text{COOH}$), and carbonyl ($-\text{CO}$) at the basal planes or edges, not only will increase the interlayer spacing to obtain single or few-layered graphene but also enables various chemical transformations and acts as anchoring sites for metal nanoparticles [3,12,13]. Nevertheless, these oxygenated species can devastate the unique properties of graphene and make it an insulator [14]. To recover the properties of graphene, GO needs to be subsequently reduced. Such post-reduced sample is designated as

* Corresponding author at. Tel.: +603 79675264; fax: +603 79675330.

E-mail address: chouyong@um.edu.my (C.Y. Tan).

<https://doi.org/10.1016/j.matresbull.2018.12.029>

Received 8 October 2018; Received in revised form 15 December 2018; Accepted 21 December 2018

Available online 21 December 2018

0025-5408/© 2018 Elsevier Ltd. All rights reserved.

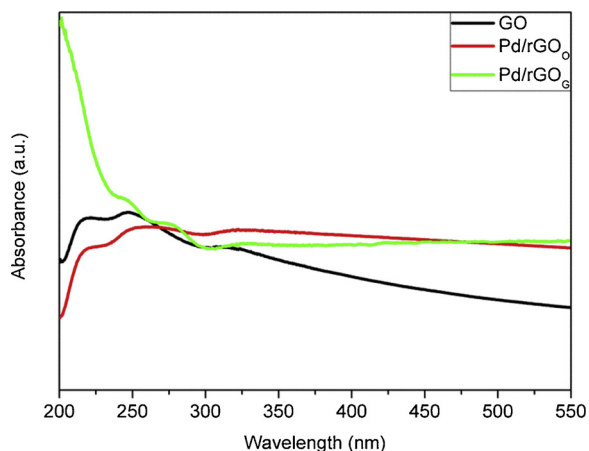


Fig. 1. UV-vis absorption spectra of GO, Pd/rGO_O, Pd/rGO_G.

reduced graphene oxide (rGO) [12].

Upon synthesis of palladium-reduced graphene oxide (Pd/rGO), the residual oxygen-containing groups serve as the depositing sites of Pd ions and nanoparticles. However, their interaction is too weak to strongly immobilize the Pd NPs, leading to irreversible agglomeration that degrades the catalytic performance [15,16]. To overcome this obstacle, various reagents have been explored. Uniformly dispersed catalyst NPs were successfully obtained on the surface of graphene sheets functionalized by branched poly(ethylenimine) [17], 1-pyrenamine [18], polydopamine [19], poly(diallyldimethylammonium chloride) [5,7], polybenzimidazole [20], and flavin mononucleotide

[21]. Some dispersing or capping agents, such as oleylamine [22], polyvinylpyrrolidone [23,24], 1-hexadecyl-2,3-dimethylimidazolium bromide [23], and trioctylphosphine [22], were also investigated. Despite the positive results, they are not without drawbacks, such as harmful, toxic, expensive or involve complex processing.

Guanine is a nucleobase found in deoxyribonucleic acid (DNA) and ribonucleic acid (RNA). Its aromatic structure allows guanine to adsorb onto graphene via π - π interaction, whereas the amino, imino, and amide groups serve to grab and control the synthesis of Pd NPs and ions. Designing an easy, fast, and scalable method to efficiently anchor Pd NPs on rGO is in great demand. To date, no study is available introducing guanine into Pd/rGO for electrooxidation of methanol for DMFC application. Our current work reported the fabrication of monodispersed Pd-guanine-rGO (Pd/rGO_G) by microwave-assisted reduction method. The electrochemical performance of the samples was studied by cyclic voltammogram (CV) and chronoamperometry (CA).

2. Materials and methods

2.1. Materials

Graphite flake (50 mesh) was purchased from Asbury Carbons. Concentrated phosphoric acid (H₃PO₄) and potassium permanganate (KMnO₄) were obtained from Wako Pure Chemical Industries, Ltd. Concentrated sulfuric acid (H₂SO₄), hydrogen peroxide (H₂O₂), fuming hydrochloric acid (HCl, 37%), palladium chloride (PdCl₂), ethylene glycol (EG), nafion, guanine, sodium hydroxide (NaOH) and potassium hydroxide (KOH) were from Sigma-Aldrich. All chemicals were analytically pure and used as received without further purification. The deionized (DI) water for solution preparation was produced from

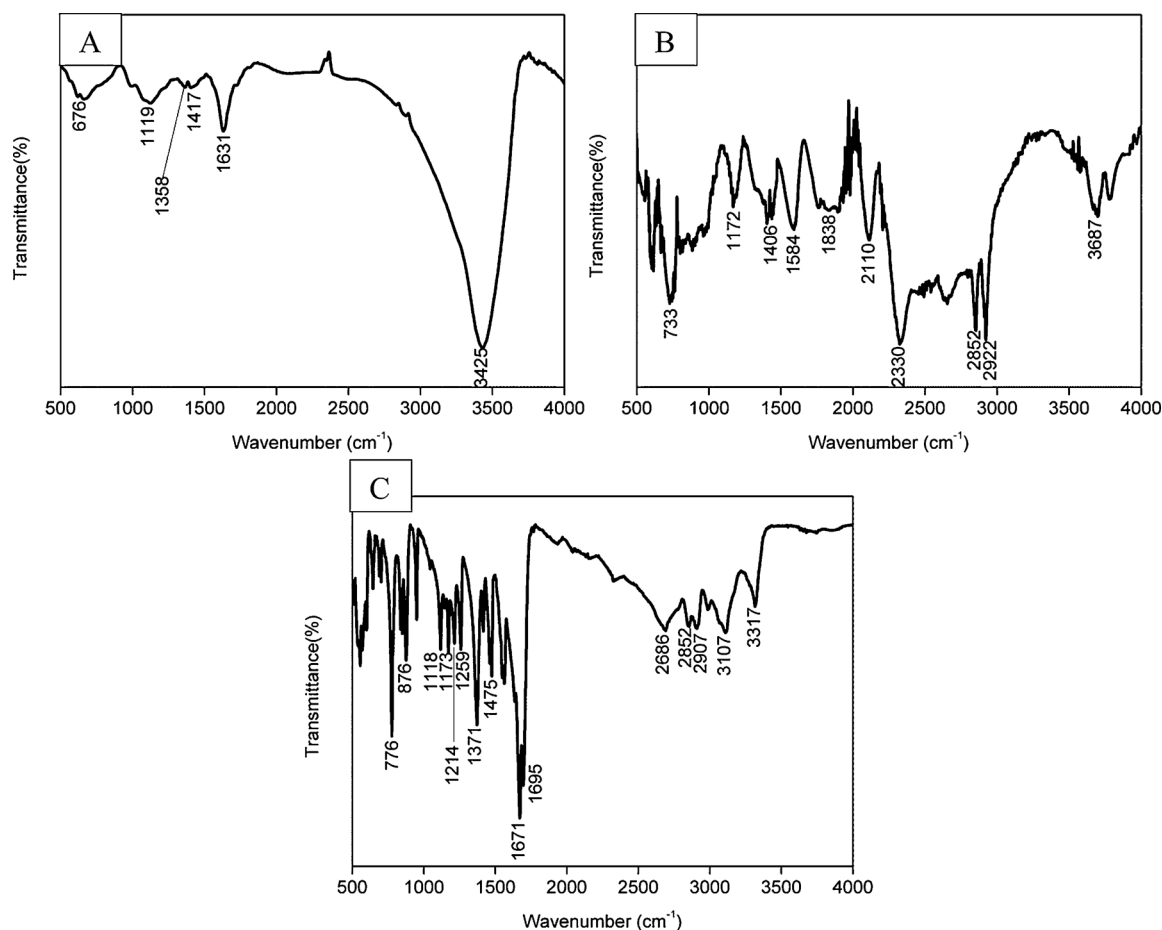


Fig. 2. FTIR spectra of (A) GO, (B) Pd/rGO_O, and (C) Pd/rGO_G.

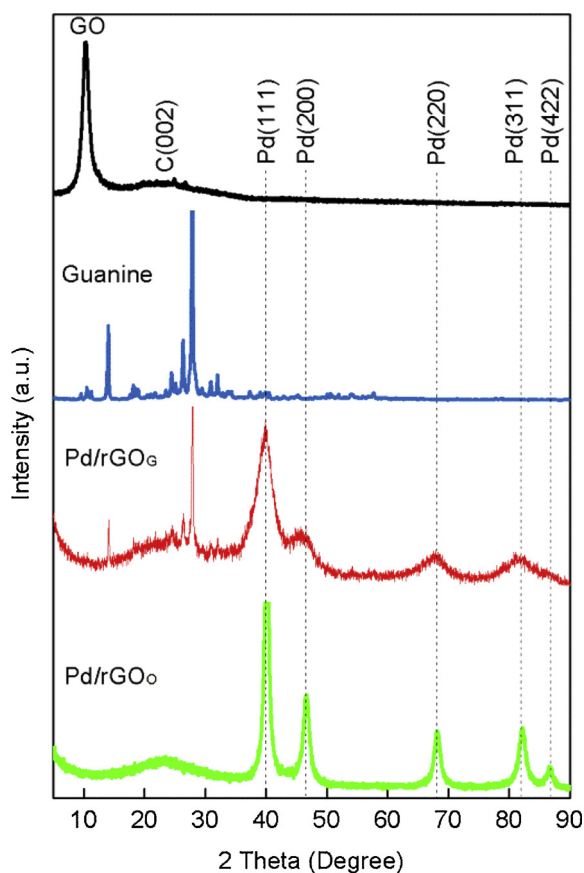


Fig. 3. XRD image of Pd/rGO_o, Pd/rGO_g, and GO.

Advantec Aquarius RFD230NA, Japan (conductivity = 0.06 μS).

2.2. Electrocatalyst synthesis

2.2.1. GO preparation

Graphite flake was oxidized to graphite oxide by improved Hummer's method published elsewhere with slight modification but the main features are briefly illustrated here [25]. H_2SO_4 was mixed with H_3PO_4 at a ratio of 360:40 mL followed by the addition of 3 g of graphite flake. Then, 18 g of KMnO_4 was added into the above mixture and stirred. After 3 days of stirring, by immersing in ice bath, 500 mL of DI water was added to the above mixture, and 17 mL of H_2O_2 was added dropwise to halt the oxidation. The mixture was then sequentially washed with 1 M of HCl thrice at 6000 rpm for 30 min by centrifuging. This process was followed up by using DI water for seven times at 10,000 rpm in 1 h. The synthesized graphite oxide was then dried overnight at 60 °C in an oven.

2.2.2. Pd/rGO_g preparation

The dried graphite oxide (120 mg) was dispersed in 80 mL of DI water and ultrasonicated for 2 h to obtain graphene oxide. Guanine (200 mg) was added and stirred for 30 min. Then, PdCl_2 (200 mg) was added and sonicated for 30 min, followed by 1 h stirring at room temperature. Upon stirring, 80 mL of EG was added dropwise. The pH of the mixture was adjusted to 10 by 1 M of NaOH. Subsequently, the mixture was reduced using a microwave at 700 W for 700 s. Finally, the resulting black solid powders were washed by DI water thrice via centrifugation at 6000 rpm for 30 min. The samples were dried overnight in an oven at 60 °C. In order to investigate the contribution of guanine to the electrooxidation of methanol, the synthesis was repeated at the absence of Pd. For comparison, conventional Pd/rGO, designated as Pd/rGO_o, was synthesized by similar procedure without guanine addition.

2.3. Characterization

The adsorption of guanine on the surface of rGO was proven by ultraviolet-visible spectroscopy (UV-vis, PerkinElmer Spectrum 400), Fourier transform infrared (FTIR) spectroscopy (Shimadzu TCC-240 A), and X-ray photoelectron spectroscopy (XPS) (ULVAC-PHI Quantera II). The characterization of morphologies and compositions of the samples were performed by field-emission scanning electron microscopy (FESEM) (HITACHI S-4800), transmission electron microscopy (TEM), and high-resolution transmission electron microscopy (HRTEM) coupled with energy-dispersive X-ray spectroscopy (FEI Tecnai F20). Raman analysis was used to investigate the defect levels, crystallinity, and structure. The procedure was performed by a JASCO NRS-3100 equipped with a charge-coupled-device detector by using argon ion at a wavelength of 532 nm. The crystallite structures were investigated by X-ray diffraction (XRD) by using an Ultima IV X-ray Diffractometer (Rigaku, America) with a Cu X-ray source ($\lambda = 0.1541$ nm) operating at 40 kV and 40 mA.

2.4. Electrochemical measurement

All the electrochemical experiments were examined with a conventional three-electrode electrochemical cell (Solartron 1280C with computerized control by ZPlot software) at room temperature. A platinum sheet of 1 cm^2 , Ag/AgCl (3 M KCl) electrode, and glassy carbon electrode (GCE, 3.0 mm diameter) were used as counter, reference, and working electrodes, respectively.

To prepare the working electrode, 2 mg as-prepared catalysts were first dispersed in 1 mL DI water and ultrasonicated for 30 min. Then, 10 μL of the suspension was casted onto the surface of polished GCE and dried in an oven at 60 °C. Subsequently, 5 μL of Nafion (0.05 wt%) was added onto the electrode surface and dried at 60 °C in the oven.

The electrochemically active surface area (ECSA) of each electrocatalyst was conducted by CV measurement in a solution of 1 M KOH from -1.0 V to 0.6 V vs. Ag/AgCl. Meanwhile, methanol oxidation activity was investigated by CV measurements in 1 M KOH + 1 M methanol at similar potential range. All the electrochemical tests were carried out at a scan rate of 50 mV s^{-1} for 10 runs. CA measurements were studied in the same methanol-contained KOH solution at an applied voltage of -0.2 V for 1000s. Electrolytes were all purged with N_2 gas for 30 min to remove any dissolved oxygen prior to the measurements.

3. Results and discussion

3.1. Characterization

Guanine adsorption on rGO is examined by UV-vis spectroscopy. As observed in Fig. 1, two UV-vis absorption peaks of GO occurred at 220 and 247 nm corresponding to the π - π^* transition of the aromatic ring C=C. A shoulder peak can also be observed at 310 nm caused by the n - π^* transition of C=O bonds. Upon formation of the nanocomposite Pd/rGO_o, the peaks red-shift to 223, 258, and 322 nm. This phenomenon signifies the successful reduction of GO and the restoration of the electronic conjugation of graphene. The further shift of Pd/rGO_g peaks to 245, 273, and 327 nm provides persuasive evidence on the co-ordination of guanine with rGO via π - π interactions as the guanine is characterized by the peaks at 248, 275, and 322 nm [26].

The nanocomposites are further characterized by FTIR analysis. FTIR spectrometry of GO, Pd/rGO_o, and Pd/rGO_g is demonstrated in Fig. 2A–C, respectively. The peaks of GO at 676, 1119, 1631, and 3425 cm^{-1} are attributed to the C=C bending vibration, C–O stretching vibration of alkoxy groups, C=C stretching vibration, and O–H group stretching vibration of phenols, respectively. Meanwhile, the peaks at 1358 and 1417 cm^{-1} can be ascribed to the O–H bending vibrations of phenols. For sample Pd/rGO_o, peaks related to oxygen

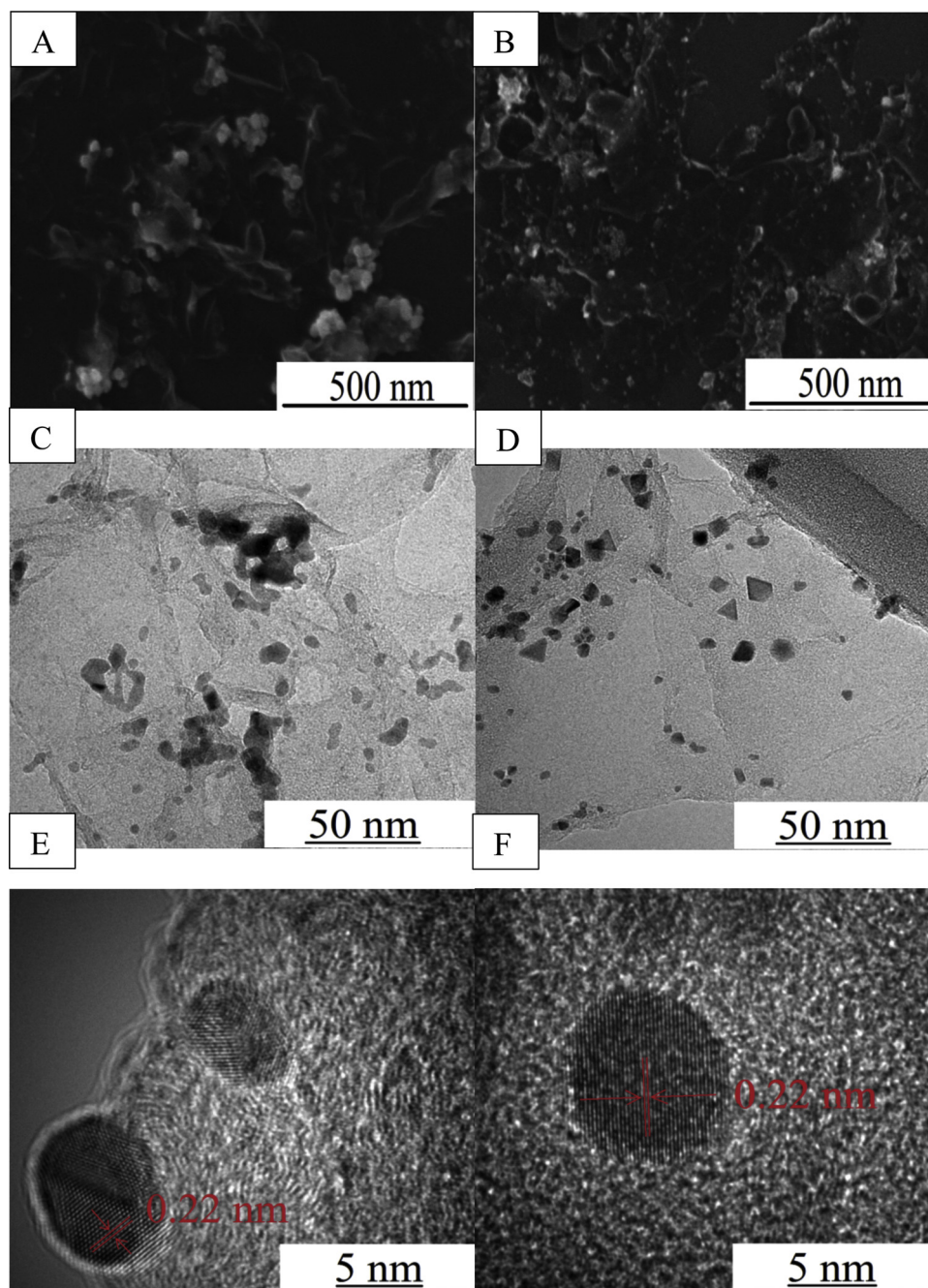


Fig. 4. FESEM images of (A) Pd/rGO₀ and (B) Pd/rGO₆. TEM images of (C) Pd/rGO₀ and (D) Pd/rGO₆. HRTEM images of (E) Pd/rGO₀ and (F) Pd/rGO₆.

functional groups, such as C–O stretching vibration (1172 cm^{-1}), O–H bending vibration (1406 cm^{-1}), and O–H stretching vibration (3687 cm^{-1}), exhibit reduced intensities, indicating rGO formation. The low intensity peaks ranging from $580\text{--}780\text{ cm}^{-1}$ and at approximately 800 cm^{-1} belong to the vibrations of the C–H bonds of the benzene rings and C–H out of plane bending vibration, respectively. As for Pd/rGO₆, a much decreased intensity of O–H stretching vibration occurs at 3107 cm^{-1} . New peaks of N–H stretching vibration are obtained at 3317 , 2907 , and 2852 cm^{-1} . C=N stretching vibration is noticed at 1671 cm^{-1} . Furthermore, peaks of C–N stretching vibration of amine are found at 1259 , 1214 , 1173 , and 1118 cm^{-1} . The existence of peaks of both N–H and C–N stretching vibration affirms the presence of the amide functional group. Meanwhile, peaks of C–N and C=N verify the functionalization of guanine in Pd/rGO₆.

The size and crystalline phase structures of the samples are analyzed

by XRD measurement. Fig. 3 shows that the peak of GO at 10.3° disappears, and a weak and broad C (002) peak at 24° occurs, suggesting the feasibility of microwave-assisted reduction method in reducing the GO [27]. Three representative peaks of guanine at 14.0° , 26.1° , and 27.9° can clearly be observed in the XRD spectrum of Pd/rGO₆, manifesting the adsorption of guanine on the surface of rGO. Peaks at approximately 40.1° , 46.5° , 68.2° , 82.1° , and 86.69° corresponds to the (111), (200), (220), (311), and (422) lattice planes of the face-centered cubic (fcc) crystalline structure of Pd (JCPDS No. 46-1043), respectively. Therefore, Pd NPs are loaded on rGO, forming the nanocomposites. Notably, the (111) peak shows the highest intensities, indicating that the Pd NPs are mainly growing in the (111) directions. Crystallite size of Pd is calculated by Scherrer's formula based on the Pd (220) peak and records 7.57 and 2.66 nm for Pd/rGO₀ and Pd/rGO₆, respectively.

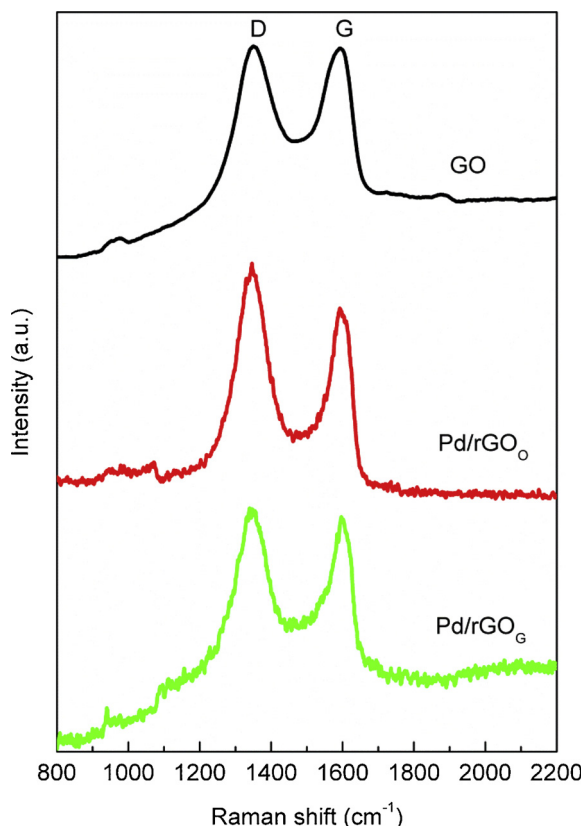


Fig. 5. Raman image of Pd/rGO_O, Pd/rGO_G, and GO.

Wrinkles and ripples induced from the GO deoxygenation are obvious for the Pd/rGO_O in Fig. 4A [28]. By contrast, Pd/rGO_G (Fig. 4B) appears slightly thickened in graphene sheets, further validating the attachment of guanine on its surface. Pd NPs with average size of 7.51 and 11.66 nm are deposited on the surface of both the functionalized and nonfunctionalized rGO, respectively. Pd NPs agglomerate in Pd/rGO_O but are uniformly dispersed with slight agglomeration for Pd/rGO_G. This observation suggests that the introduction of guanine is effective in restraining the agglomeration of Pd NPs. In contrast to the circular nanoparticles of Pd/rGO_O (Fig. 4C), various shapes, such as triangular, square, circular, and diamond shapes, are observed for Pd/rGO_G (Fig. 4D). These shapes reveal the capability of the amino, amide, and imino groups of guanine to control the synthesis of Pd NPs. HRTEM shows the lattice spacing of both samples is approximately 0.22 nm (Fig. 4E and F), conforming to the (111) planes of the fcc of Pd. The mass loadings of Pd NPs of the samples are quantified by EDX and records 73.29% and 20.61% for Pd/rGO_O and Pd/rGO_G, respectively.

Raman characterization is carried out to study the defect levels and quality of reduced graphene oxide. As shown in Fig. 5, two representative bands of graphene, D band and G band, occur at 1330–1350 cm⁻¹ and approximately 1590 cm⁻¹, respectively. The former peak is initiated by the structural disorder or intrinsic defects due to an A_{1g} vibrational mode. The latter is correlated to the first-order scattering of the E_{2g} mode of graphite that is associated to the coplanar vibration of sp²-hybridized carbon atoms in a two-dimensional hexagonal lattice [3]. The G band of Pd/rGO_O and Pd/rGO_G red-shifts from 1589 cm⁻¹ of GO to 1592 and 1598 cm⁻¹, respectively. Therefore, the GO is partially reduced, and the graphitic structure is restored. The intensity ratio of D band to G band ($\frac{I_D}{I_G}$) is a parameter to determine the degree of graphitization and defect level of carbon materials [18]. Relative to GO, $\frac{I_D}{I_G}$ increases from 1.00 to 1.05 and 1.01 for Pd/rGO_O and Pd/rGO_G, respectively. Such increase in ratio can be ascribed to the creation of defects during the reduction of GO and deposition of Pd NPs

on rGO [29,30]. The low ratio of Pd/rGO_G implies that it has high degree of graphitization and low defect density. The introduction of guanine is signified to preferably preserve the electronic structure and integrity of rGO and offers more active sites on the surface of rGO for the loading of Pd NPs. As defects on rGO serve as Nucleation Center for Clustering (NCC) for the coalescence of Pd NPs at its vicinity, agglomeration is serious in Pd/rGO_O [24].

XPS analysis is conducted to probe the chemical composition and content of Pd/rGO_G and to verify the attachment of guanine to the rGO. Fig. 6A demonstrates the XPS spectra of Pd/rGO_G. N1s peak can clearly be observed at 398 eV, signaling the functionalization of guanine on rGO. The peaks at approximately 285 eV, 340 eV, and 530 eV are the peaks of C1s, Pd3d, and O1s, respectively. The presence of Pd peak confirms the successful deposition of Pd NPs. The deconvolution of C1s XPS spectrum (Fig. 6B) shows dominant C–N bonds (285.8 eV), C–C/C=C bonds (284.7 eV), C–O bonds (286.7 eV), NH₂/N–C=O bonds (287.5 eV), and C=O bonds (288.1 eV). The C–O bonds involve hydroxyl (–OH) and epoxide (–O–); C=O bonds comprise carboxyl (–COOH), carbonyl (–C=O), and carboxylate (–COOR) [31]. The low intensity of C–O and C=O peak signifies successful reduction of GO, where a large number of oxygen-containing species of GO are removed. The existence of C–N and NH₂/N–C=O bonds indicates that guanine has been adsorbed onto the surface of rGO. In Fig. 6C, the N1s peak is deconvoluted into the peaks of –N = groups (N1) at 398.54 eV and –NH₂ bond (N2) at 399.94 eV. The former peak is resulted from the pyridinic nitrogen of guanine, whereas the latter is attributed to the amine groups. The observation in Fig. 6D, where the Pd⁰ peaks dominate in the deconvolution of the Pd3d peak, further verifies the high degree reduction of the synthesis. In brief, the findings are in accordance with the UV–vis, FTIR, XRD, and Raman results.

3.2. Electrochemical measurements

Fig. 7A and B shows the electrochemical tests to provide insight to the effect of introduction of guanine to the catalytic activity. The inset in Fig. 7A clearly reveals that the rGO and guanine can be a catalyst with the former slightly stronger than the latter. Both rGO and guanine catalyse the methanol oxidation reaction (MOR), achieving peak at –0.17 and –0.15 V vs. Ag/AgCl, respectively. Nevertheless, the standalone guanine is weak in the electrooxidation of methanol. Upon functionalization of guanine on rGO, the electrooxidation of methanol is enhanced significantly. The electrochemical performance is further boosted as high as 164% at the presence of Pd NPs. It is hypothesized that the addition of guanine to rGO leads to larger ECSA, and thus the extraordinary methanol oxidation activity of rGO + guanine. However, Fig. 7B declines the hypothesis because the introduction of guanine to rGO does not have any impact to the ECSA. Such an observation complies with the FESEM image in Fig. 5B, where the rGO become thicker at the presence of guanine. Thus, such improvement can be credited to the unique properties of graphene that facilitates the electron transfer of guanine, leading to the increase in current densities [32].

High ECSA is greatly desired for effective electron and mass transfer to and from the electrode surface [11,12]. The ECSA is calculated from the area of reduction peak of palladium oxide (PdO) in the potential region of –0.7 to –0.2 V vs. Ag/AgCl on the CV in Fig. 8(A) according to the following equation [33]:

$$ECSA = \frac{Q}{SI}$$

where “Q” is the coulombic charge (mC) for the PdO reduction; “S” is a conversion factor corresponding to 0.424 mC cm⁻², and “I” is the mass of catalyst (mg) loaded on the GCE [33]. The Pd/rGO_O and Pd/rGO_G attain ECSA values of 63.80 and 111.98 m² g⁻¹, respectively. In the discussion above, the introduction of guanine does not contribute to the ECSA of rGO. Therefore, the increased ECSA is mainly from the Pd NPs.

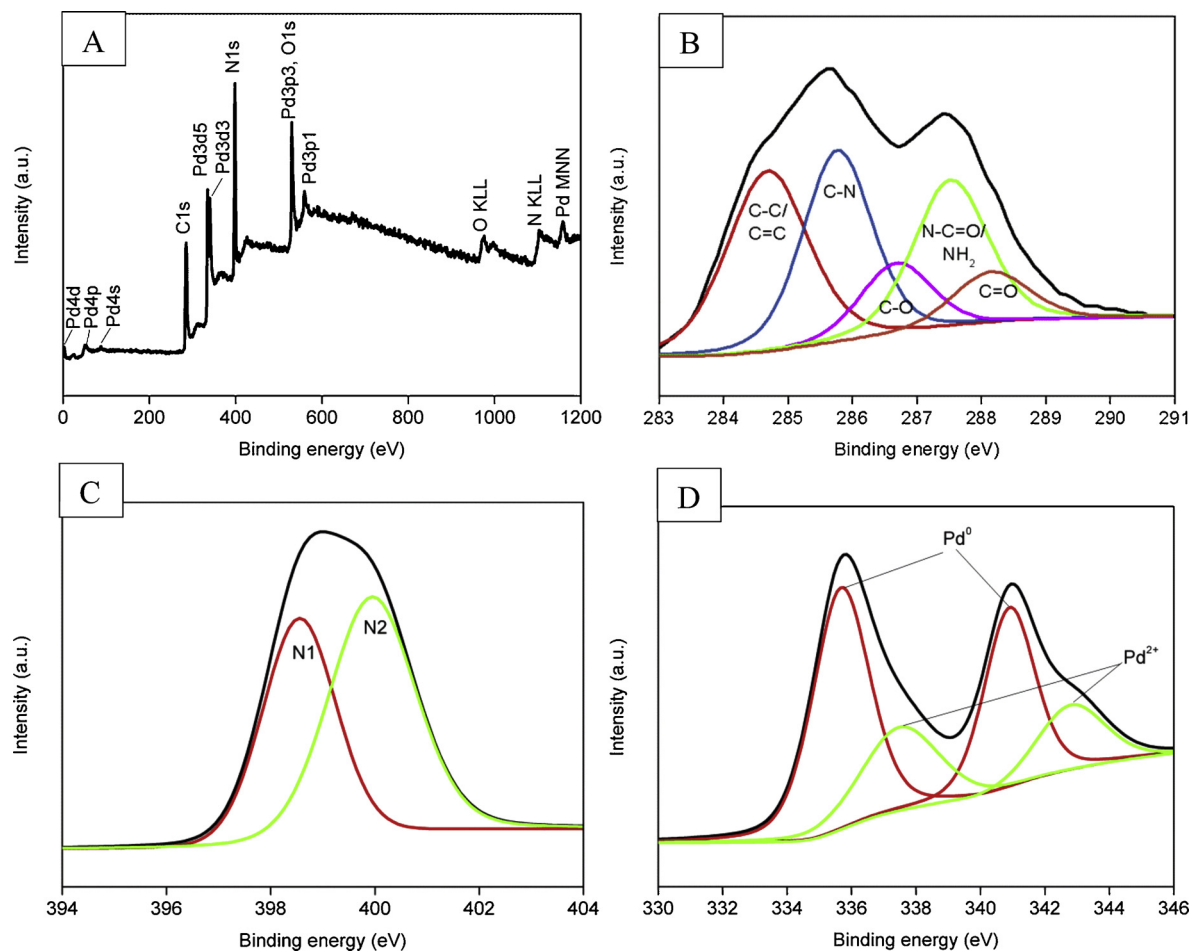


Fig. 6. XPS spectrum of (A) Pd/rGO_G. Deconvolution of the high resolution XPS spectra of (B) C1s, (C) N1s, and (D) Pd3d in Pd/rGO_G.

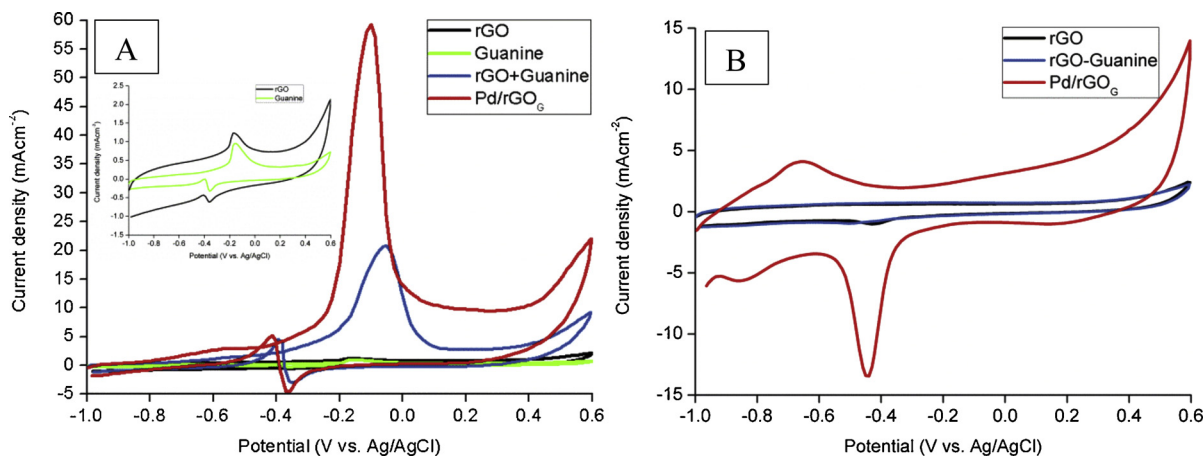


Fig. 7. (A) The cyclic voltammogram of rGO, rGO + guanine, and Pd/rGO_G in nitrogen saturated solutions of 1 M KOH. (Inset of (A) is magnified cyclic voltammogram of rGO and guanine). (B) The cyclic voltammogram of rGO, rGO + guanine, and Pd/rGO_G in nitrogen saturated solutions of 1 M KOH/ 1 M CH₃OH with scan rate of 50 mV s⁻¹.

Evidently, the small size and uniform dispersion of Pd NPs are the governing factors to the great ECSA of the Pd/rGO_G.

As shown in Fig. 8(B), Pd/rGO_G reports 183% improvement in MOR (1017.42 mA mg⁻¹ vs. 359.80 mA mg⁻¹). Despite the almost similar onset potential (E_{onset} ; -0.44 vs. -0.43 V vs. Ag/AgCl), the incorporation of guanine favours negative half-wave potential ($E_{1/2}$; -0.18 vs. -0.12 V vs. Ag/AgCl) and peak potential (E_{peak} ; -0.10 vs. -0.07 V vs. Ag/AgCl). Such an outcome can be attributed to the combination of the catalytic capabilities of Pd NPs, guanine, and rGO.

Certainly, the evenly dispersed small Pd NPs and great ECSA also play a part. Notably, Pd/rGO_G is significantly more promising than the reported commercial Pd/C (107.8 A g⁻¹) [34]. A promising electrocatalyst can also be defined by its ability to resist poisoning of intermediate species particularly CO that can be embodied by the ratio of forward to backward peak current density, I_f/I_b [35,36]. In this context, Pd/rGO_G records much higher ratio (11.38) compared with Pd/rGO_O (3.98). Therefore, Pd/rGO_G has better capability to facilitate the oxidation of CO to carbon dioxide, re-exposing the active sites.

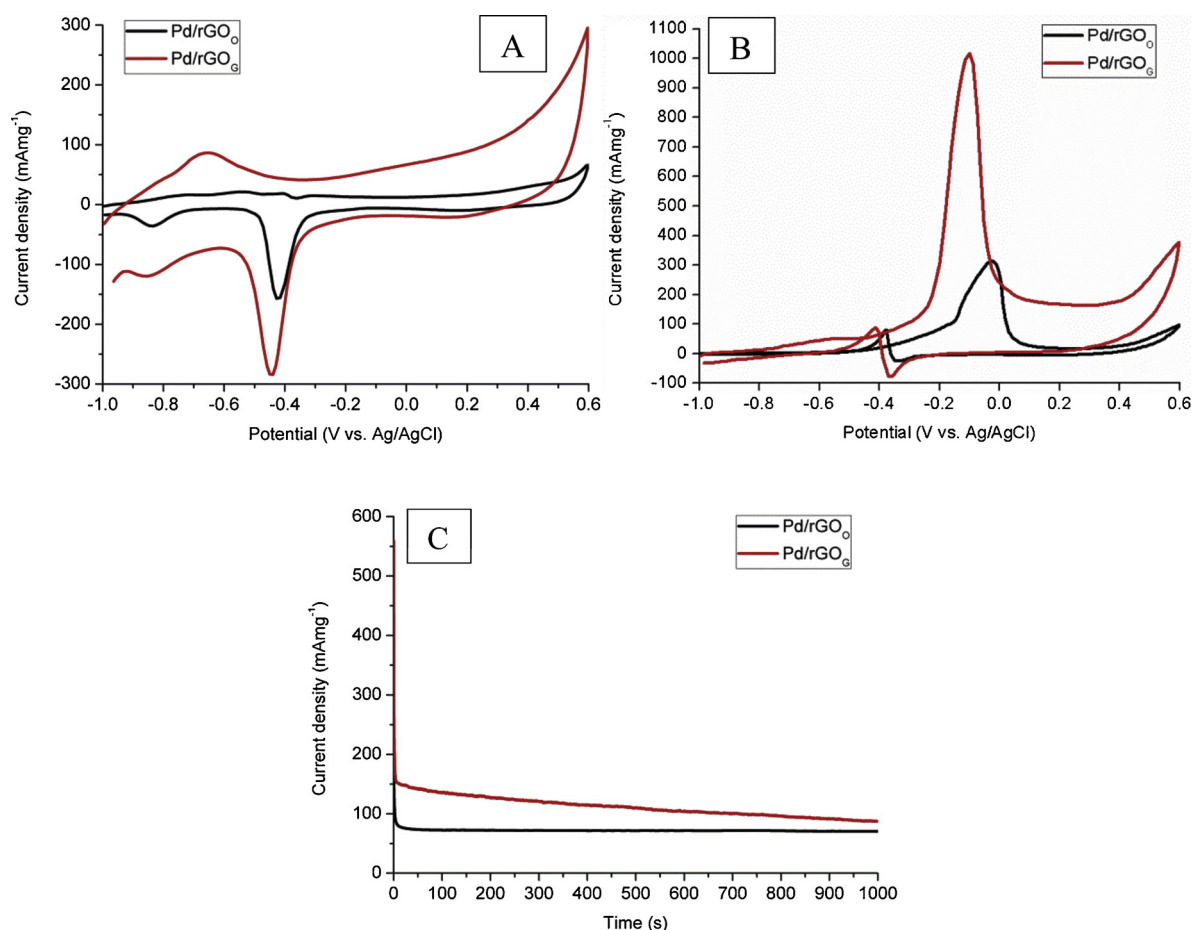


Fig. 8. The cyclic voltammogram of Pd/rGO₀ and Pd/rGO₆ in nitrogen saturated solutions of (A) 1 M KOH and (B) 1 M KOH/ 1 M CH₃OH with scan rate of 50 mV s⁻¹. (C) The chronoamperogram of Pd/rGO₀ and Pd/rGO₆ in nitrogen saturated solutions of 1 M KOH/ 1 M CH₃OH with scan rate of 50 mV s⁻¹ at an applied potential of -0.2 V vs. Ag/AgCl.

In term of the stability of electrocatalysts (Fig. 8(C)), Pd/rGO₆ retains high current density (87.36 mA mg⁻¹ vs 70.56 mA mg⁻¹). Both electrocatalysts undergo rapid degradation in MOR performance during the first 50 s due to the formation of intermediate species [37,38]. Further continuous operation oxidizes the intermediate species, liberating the active sites and thus the subsequent steady drop in current density. The good stability of Pd/rGO₆ can be reasoned by its high graphitization level and low defect density. Defects can promote the corrosion of electrocatalysts under electrochemical operation. Small particle size, uniform distribution, and large ECSA are other contributing factors.

4. Conclusions

This work designs a straightforward and novel method to introduce safe and cost-effective guanine into Pd/rGO. The abundant amino, imino, and amide groups of guanine enable the immobilization of the Pd NPs and ions, restricting their agglomeration. The aromatic structure of guanine interacts with rGO via π - π interaction. The results reveal the capability of guanine to direct the structure of Pd NPs, attaining triangular, rectangular, circular, and diamond shapes. Guanine is also discovered to have catalytic effect toward MOR. Therefore, the guanine can be a second catalyst. The as-synthesized Pd/rGO₆ exhibits significant enhanced MOR (1017.42 mA mg⁻¹ vs. 359.80 mA mg⁻¹, 183% improvement), good durability, and more negative half-wave and peak potential. This new nanocomposite obtains slightly better tolerance to the poisoning intermediate species. Such promising enhancement can be credited to the small particle size and uniform dispersion of Pd NPs

that increase the active catalytic sites for electrochemical reaction. In summary, Pd/rGO₆ is a remarkable anodic electrocatalysts for DMFCs.

Acknowledgements

This study was supported under the Frontier Research Grant grant number FG0011-17AFR, Postgraduate Research Grant (PPP) grant number PG207-2015A, Talent Fund of South China University of Technology and Nippon Sheet Glass Foundation for Materials Science and Engineering (NSG Foundation) research grant no. IF014-2017. The authors gratefully acknowledge AUN/SEED-Net, JICA, University of Malaya and the Ministry of Higher Education Malaysia for the financial support.

References

- [1] Y. Zhang, G. Chang, H. Shu, M. Oyama, X. Liu, Y. He, Synthesis of Pt-Pd bimetallic nanoparticles anchored on graphene for highly active methanol electro-oxidation, *J. Power Sources* 262 (2014) 279–285.
- [2] L. Lin, M. Li, L. Jiang, Y. Li, D. Liu, X. He, L. Cui, A novel iron (II) polyphthalocyanine catalyst assembled on graphene with significantly enhanced performance for oxygen reduction reaction in alkaline medium, *J. Power Sources* 268 (2014) 269–278.
- [3] J. Zhao, H. Li, Z. Liu, W. Hu, C. Zhao, D. Shi, An advanced electrocatalyst with exceptional electrocatalytic activity via ultrafine Pt-based trimetallic nanoparticles on pristine graphene, *Carbon* 87 (2015) 116–127.
- [4] L. Gong, Z. Yang, K. Li, J. Ge, C. Liu, W. Xing, Recent development of methanol electrooxidation catalysts for direct methanol fuel cell, *J. Energy Chem.* 27 (2018) 1618–1628.
- [5] Y. Fan, Y. Zhao, D. Chen, X. Wang, X. Peng, J. Tian, Synthesis of Pd nanoparticles supported on PDDA functionalized graphene for ethanol electro-oxidation, *Int. J. Hydrogen Energy* 40 (1) (2015) 322–329.

- [6] L. Li, M. Chen, G. Huang, N. Yang, L. Zhang, H. Wang, Y. Liu, W. Wang, J. Gao, A green method to prepare Pd–Ag nanoparticles supported on reduced graphene oxide and their electrochemical catalysis of methanol and ethanol oxidation, *J. Power Sources* 263 (2014) 13–21.
- [7] M. Zhang, Y. Li, Z. Yan, J. Jing, J. Xie, M. Chen, Improved catalytic activity of cobalt core–platinum shell nanoparticles supported on surface functionalized graphene for methanol electro-oxidation, *Electrochim. Acta* 158 (2015) 81–88.
- [8] D. Chen, L. Tang, J. Li, Graphene-based materials in electrochemistry, *Chem. Soc. Rev.* 39 (8) (2010) 3157–3180.
- [9] L. Tang, Y. Wang, Y. Li, H. Feng, J. Lu, J. Li, Preparation, structure, and electrochemical properties of reduced graphene sheet films, *Adv. Funct. Mater.* 19 (17) (2009) 2782–2789.
- [10] A. Esmaeili, M.H. Entezari, Facile and fast synthesis of graphene oxide nanosheets via bath ultrasonic irradiation, *J. Colloids Interface Sci.* 432 (2014) 19–25.
- [11] J.-N. Zheng, S.-S. Li, F.-Y. Chen, N. Bao, A.-J. Wang, J.-R. Chen, J.-J. Feng, Facile synthesis of platinum–ruthenium nanodendrites supported on reduced graphene oxide with enhanced electrocatalytic properties, *J. Power Sources* 266 (2014) 259–267.
- [12] C.-T. Hsieh, J.-L. Gu, Y.-C. Chen, D.-Y. Tzou, Pulse microwave synthesis of palladium catalysts on graphene electrodes for proton exchange membrane fuel cells, *Electrochim. Acta* 98 (2013) 39–47.
- [13] S. Wang, P.-J. Chia, L.-L. Chua, L.-H. Zhao, R.-Q. Png, S. Sivaramakrishnan, M. Zhou, R.G.S. Goh, R.H. Friend, A.T.S. Wee, P.K.H. Ho, Band-like transport in surface-functionalized highly solution-processable graphene nanosheets, *Adv. Mater.* 20 (18) (2008) 3440–3446.
- [14] A.A. Ensaifi, M. Jafari-Asl, B. Rezaei, A new strategy for the synthesis of 3-D Pt nanoparticles on reduced graphene oxide through surface functionalization, application for methanol oxidation and oxygen reduction, *Electrochim. Acta* 130 (2014) 397–405.
- [15] X. Li, S. Ci, J. Jia, Z. Wen, Graphene loading molybdenum carbide/oxide hybrids as advanced electrocatalysts for hydrogen evolution reaction, *Int. J. Hydrogen Energy* 41 (46) (2016) 21246–21250.
- [16] R. Kou, Y. Shao, D. Mei, Z. Nie, D. Wang, C. Wang, V.V. Viswanathan, S. Park, I.A. Aksay, Y. Lin, Y. Wang, J. Liu, Stabilization of electrocatalytic metal nanoparticles at metal–metal oxide–graphene triple junction points, *J. Am. Chem. Soc.* 133 (8) (2011) 2541–2547.
- [17] Z. Lv, X. Yang, E. Wang, Highly concentrated polycations-functionalized graphene nanosheets with excellent solubility and stability, and its fast, facile and controllable assembly of multiple nanoparticles, *Nanoscale* 5 (2) (2013) 663–670.
- [18] L. Li, J. Zhang, Y. Liu, W. Zhang, H. Yang, J. Chen, Q. Xu, Facile fabrication of Pt nanoparticles on 1-pyrenamine functionalized graphene nanosheets for methanol electrooxidation, *ACS Sustain. Chem. Eng.* 1 (5) (2013) 527–533.
- [19] W. Ye, Y. Chen, Y. Zhou, J. Fu, W. Wu, D. Gao, F. Zhou, C. Wang, D. Xue, Enhancing the catalytic activity of flowerlike Pt nanocrystals using polydopamine functionalized graphene supports for methanol electrooxidation, *Electrochim. Acta* 142 (2014) 18–24.
- [20] L. Xin, F. Yang, Y. Qiu, A. Uzunoglu, T. Rockward, R.L. Borup, L.A. Stanciu, W. Li, J. Xie, Polybenzimidazole (PBI) functionalized nanographene as highly stable catalyst support for polymer electrolyte membrane fuel cells (PEMFCs), *J. Electrochem. Soc.* 163 (10) (2016) F1228–F1236.
- [21] M. Ayán-Varela, R. Ruiz-Rosas, S. Villar-Rodil, J.I. Paredes, D. Cazorla-Amorós, E. Morallón, A. Martínez-Alonso, J.M.D. Tascón, Efficient Pt electrocatalysts supported onto flavin mononucleotide–exfoliated pristine graphene for the methanol oxidation reaction, *Electrochim. Acta* 231 (2017) 386–395.
- [22] S. Yang, J. Dong, Z. Yao, C. Shen, X. Shi, Y. Tian, S. Lin, X. Zhang, One-pot synthesis of graphene-supported monodisperse Pd nanoparticles as catalyst for formic acid electro-oxidation, *Sci. Rep.* (2014) 4.
- [23] J.-J. Lv, S.-S. Li, A.-J. Wang, L.-P. Mei, J.-J. Feng, J.-R. Chen, Z. Chen, One-pot synthesis of monodisperse palladium–copper nanocrystals supported on reduced graphene oxide nanosheets with improved catalytic activity and methanol tolerance for oxygen reduction reaction, *J. Power Sources* 269 (2014) 104–110.
- [24] C.A. Martins, P.S. Fernández, F. de Lima, H.E. Troiani, M.E. Martins, A. Arenillas, G. Maia, G.A. Camara, Remarkable electrochemical stability of one-step synthesized Pd nanoparticles supported on graphene and multi-walled carbon nanotubes, *Nano Energy* 9 (2014) 142–151.
- [25] J. Chen, B. Yao, C. Li, G. Shi, An improved Hummers method for eco-friendly synthesis of graphene oxide, *Carbon* 64 (2013) 225–229.
- [26] V.L. Chandraboss, B. Karthikeyan, S. Senthilvelan, Experimental and first-principles investigation of the adsorption and entrapment of guanine with SiO₂ clusters of sol-gel silicate material for understanding DNA photodamage, *Phys. Chem. Chem. Phys.* 17 (18) (2015) 12100–12114.
- [27] A.H.M. Videla, S. Ban, S. Specchia, L. Zhang, J. Zhang, Non-noble Fe–NX electrocatalysts supported on the reduced graphene oxide for oxygen reduction reaction, *Carbon* 76 (2014) 386–400.
- [28] R.P. Antony, L.K. Preethi, B. Gupta, T. Mathews, S. Dash, A.K. Tyagi, Efficient electrocatalytic performance of thermally exfoliated reduced graphene oxide–Pt hybrid, *Mater. Res. Bull.* 70 (Supplement C) (2015) 60–67.
- [29] Z. Ji, X. Shen, Y. Xu, G. Zhu, K. Chen, Anchoring noble metal nanoparticles on CeO₂ modified reduced graphene oxide nanosheets and their enhanced catalytic properties, *J. Colloids Interface Sci.* 432 (Supplement C) (2014) 57–64.
- [30] D.-J. Chen, Q.-L. Zhang, J.-X. Feng, K.-J. Ju, A.-J. Wang, J. Wei, J.-J. Feng, One-pot wet-chemical co-reduction synthesis of bimetallic gold–platinum nanochains supported on reduced graphene oxide with enhanced electrocatalytic activity, *J. Power Sources* 287 (Supplement C) (2015) 363–369.
- [31] L. Zhao, Z.-B. Wang, J.-L. Li, J.-J. Zhang, X.-L. Sui, L.-M. Zhang, Hybrid of carbon-supported Pt nanoparticles and three dimensional graphene aerogel as high stable electrocatalyst for methanol electrooxidation, *Electrochim. Acta* 189 (2016) 175–183.
- [32] J. Tang, L. Hou, D. Tang, J. Zhou, Z. Wang, J. Li, G. Chen, Magneto-controlled electrochemical immunoassay of brevetoxin B in seafood based on guanine-functionalized graphene nanoribbons, *Biosens. Bioelectron.* 38 (1) (2012) 86–93.
- [33] J. Qi, N. Benipal, C. Liang, W. Li, PdAg/CNT catalyzed alcohol oxidation reaction for high-performance anion exchange membrane direct alcohol fuel cell (alcohol = methanol, ethanol, ethylene glycol and glycerol), *Appl. Catal. B: Environ.* 199 (Supplement C) (2016) 494–503.
- [34] L. Yang, D. Yan, C. Liu, H. Song, Y. Tang, S. Luo, M. Liu, Vertically oriented reduced graphene oxide supported dealloyed palladium–copper nanoparticles for methanol electrooxidation, *J. Power Sources* 278 (2015) 725–732.
- [35] H. Feng, Y. Liu, J. Li, Highly reduced graphene oxide supported Pt nanocomposites as highly efficient catalysts for methanol oxidation, *Chem. Commun.* 51 (12) (2015) 2418–2420.
- [36] Y.-C. Shi, L.-P. Mei, A.-J. Wang, T. Yuan, S.-S. Chen, J.-J. Feng, L-Glutamic acid assisted eco-friendly one-pot synthesis of sheet-assembled platinum–palladium alloy networks for methanol oxidation and oxygen reduction reactions, *J. Colloid Interface Sci.* 504 (2017) 363–370.
- [37] Y. Li, L. Tang, J. Li, Preparation and electrochemical performance for methanol oxidation of Pt/graphene nanocomposites, *Electrochem. Commun.* 11 (4) (2009) 846–849.
- [38] L. Zhang, X.-F. Zhang, X.-L. Chen, A.-J. Wang, D.-M. Han, Z.-G. Wang, J.-J. Feng, Facile solvothermal synthesis of Pt₇₁Co₂₉ lamellar nanoflowers as an efficient catalyst for oxygen reduction and methanol oxidation reactions, *J. Colloid Interface Sci.* 536 (2019) 556–562.